AIAA'87

AIAA-87-1872
Pressure Oscillations and Acoustic-Entropy Interactions in Ramjet Combustion Chambers

J.W. Humphrey and F.E.C. Culick,
California Inst. of Technology,
Pasadena, CA

AIAA/SAE/ASME/ASEE 23rd Joint Propulsion Conference

June 29-July 2, 1987/San Diego, California

PRESSURE OSCILLATIONS AND ACOUSTIC-ENTROPY INTERACTIONS IN RAMJET COMBUSTION CHAMBERS

Joseph W. Humphrey* and F.E.C. Culick**
California Institute of Technology
Pasadena, California

March 26, 1987

Abstract

A one-dimensional analytical model is presented for calculating the longitudinal acoustic modes of idealized "dump-type" ramjet engines. The model contains the matching required to place an oscillating flame sheet in the interior of a combustion chamber with mean flow. The linear coupling of the acoustic and entropy waves at the inlet shock, flame sheet, and exit nozzle along with acoustic admittances at the inlet and exit are combined to determine the stability of the system as well as the acoustic modes. Since the acoustic and entropy waves travel at different velocities, the geometry is a critical factor in determining stability. Typical values of the admittances will produce damped solutions when the entropy is neglected, but, as the ratio of the entropy to acoustic fluctuations is increased, the coupling can either feed acoustic energy into or out of different modes independently. This transfer of energy has a destabilizing or stabilizing effect on the acoustic modes of the system depending upon the phase of the energy transfer.

1 Introduction

Renewed interest in ramjet engine applications has led to new efforts to study pressure oscillations (or combustion instabilities) in ramjet combustors. When pressure oscillations occur in ramjet combustion chambers, they usually fall into two categories: low frequency oscillations and high frequency oscillations. The low frequency modes are associated with the longitudinal modes of the system and typically range from 50 to 600 Hertz. The high frequency oscillations are associated with the transverse and radial modes of the chamber and range from 2000 to 5000 Hertz. Davis [1] found experimentally that for a test dump combustor the amplitudes of the high frequency modes was relatively small. This study deals with the low frequency modes.

* Member AIAA, currently at Aerojet Propulsion Research Institute.
** Professor of Jet Propulsion and Applied Physics, Associate Fellow AIAA.

Two recent experimental studies of combustion instabilities with flow visualization (Smith [2] and Davis [1]) have indicated the flow out of a combustor may contain significant temperature fluctuations. In an attempt to predict the stability of these systems, the influence and importance of entropy has been studied. Specifically, the way in which entropy fluctuations influence the stability of oscillatory longitudinal acoustic modes of the combustor.

The linear coupling of acoustics with entropy can provide the mechanism through which energy transfer can influence stability. Three specific mechanisms of coupling are used in the combustor modeling. Chu [3]-[6] developed a plane flame matching condition for a constant area normal deflagration. Marble and Candel [7] studied the reflectance of incident entropy waves as pressure waves from choked exit nozzles. Culick and Rogers [8] investigated the response of an oscillating inlet diffuser shock. Each of these analyses contain linear acoustic-entropy interactions and model acoustically compact processes that occur in typical dump ramjet combustor configurations. The stability of pressure oscillations is examined with coupling at the inlet entrance, at the mean flame location, and at the exit nozzle. Stability will be shown to be dependent on the phase of the entropy relative to pressure at each of the three coupling points. When the geometry produces "in phase" coupling, then driving will occur which can sometimes overcome losses and result in linear instability. Similarly, "out of phase" coupling will remove energy from the oscillation.

2 Analysis

The low frequency, longitudinal acoustic modes are predominantly one-dimensional and are treated here in one-dimension only. The equations of motion in one-dimension, neglecting heat-conduction and dissipation are

$$P_t + uP_x + \gamma P u_x = a_0 w + \frac{Pq}{\gamma}, \qquad (1)$$

$$u_t + uu_x + \frac{a^2}{\gamma P} P_x = b_f, \qquad (2)$$

$$s_t + us_x = q, \qquad (3)$$

where w, b_f, and q are mass, body force, and entropy sources. The sonic velocity is $a^2 = \sqrt{\gamma RT}$. The linearized equations of combined acoustics and entropy are obtained by writing the dependent variables as sums of mean and fluctuating values (i.e. $u(x,t) = u_0(x) + u'(x,t)$, etc.) and substitution into 1-3. Linearize the equations of motion in the absence of sources to find

$$\rho u'_t + \rho u u'_x + p'_x = 0, \quad (4)$$

$$P'_t + u P'_x + \gamma P u'_x = 0, \quad (5)$$

$$s'_t + u s'_x = 0, \quad (6)$$

where the unprimed quantities are understood to be mean quantities. For constant area flows without distributed losses, the mean flow is uniform. When the time dependence is assumed to be periodic, the general solution to 4-6 is given by

$$P'(x,t) = P_0\left[P^+ e^{iKx} + P^- e^{-iKx}\right] e^{-iM_0 Kx} e^{-i\Omega t}, \quad (7)$$

$$u'(x,t) = \frac{P_0}{\rho_0 a_0}\left[P^+ e^{iKx} - P^- e^{-iKx}\right] e^{-iM_0 Kx} e^{-i\Omega t} \quad (8)$$

$$s'(x,t) = A e^{i\frac{\Omega}{u_0}x} e^{-i\Omega t}, \quad (9)$$

(10)

where

$$K = \frac{k}{1 - M_0^2}, \quad M_0 = \frac{u_0}{a_0}, \quad k = \frac{\Omega}{a_0}, \quad \Omega = \omega + i\alpha. \quad (11)$$

The model geometry is given in Figure 1. The inlet boundary is terminated upstream by an inlet reflectance and inlet acoustic-entropy interaction. The inlet boundary conditions can be either given or calculated from the inlet shock admittance theory of Culick and Rogers.[8] The inlet is a simple constant area channel connected to the combustor by an abrupt dump plane. The combustor is divided into two sections of constant area channel that are coupled across a plane flame. The exit end of the combustor is terminated with a choked exit nozzle. Each of the boundaries and matching conditions are treated as acoustically compact due to the long wavelengths of the low frequencies.

2.1 Inlet Boundary Conditions

There are two components of the inlet boundary condition: an acoustic reflectance and an acoustic-entropy coupling relation. If the inlet reflectance (that is, the reflectance of a leftward traveling acoustic wave in the combustor at the inlet end of the combustor) is known, then it can simply be used. The inlet, however, may be a dump plane, which is then connected to an inlet duct. The inlet duct may in turn be terminated with a choked inlet diffuser as in a missile application. In a connected pipe experiment, however, the inlet duct may be connected by another dump plane to a plenum chamber and so on back upstream. Since this case is subsonic, it is not decoupled and is part of the acoustic system. It is the resonance of this system which is important.

The inlet duct is treated as an acoustic region and is coupled to the combustor acoustic region by matching conditions. Typically the matching condition at a dump plane is continuity of mass and pressure, while the expansion is treated as nearly isentropic. Thus the inlet boundary condition is replaced by matching conditions and an upstream inlet duct boundary condition. This process can be repeated until each acoustic element has been accounted for with matching conditions and a new boundary condition.

The specific geometries of interest are shown in Figure 1. The first two are useful in analyzing experimental tests that are not terminated by an inlet diffuser shock. The third geometry is useful in analyzing actual applications as well as experimental tests which have inlet shock waves. The shock wave plays an important role in defining the acoustic system because it clearly defines the upstream boundary. No acoustic waves can penetrate a shock wave since the acoustic velocity is less than the flow entering the shock.

The shock wave also has characteristics which are significantly different from the geometry shown in Figure 1 (Geometry 1). The acoustic energy is not dissipated by the acoustic wall, plenum, plenum-inlet dump, inlet duct, and inlet-combustor dump of Geometry 1. No significant entropy fluctuation is generated upstream of the combustor in this geometry either. The inlet shock on the other hand, absorbs about ninety percent of the incident acoustic energy and generates an upstream fluctuating entropy. As a result, the *system* acoustics are significantly different.

Since these equations are linear, it is possible to define a reflectance at the combustor inlet that contains all of the upstream conditions. This is the procedure adopted here. If this is not done, then a more complex transcendental equation for the resonant frequencies must be solved, although the results are the same. The following sections develop the inlet conditions for Geometry 3 in Figure 1 which will be used in the combustor modeling.

2.1.1 Calculation of Reflectance

Calculate $\beta_I = P_1^+/P_1^-$ and A/P_1^- for the geometry shown in Figure 2. The inlet shock, diffuser, inlet duct, and inlet-combustor dump plane are used to determine the combustor inlet reflectance β_I and entropy A/P_1^-.

Region D

$$P'_d(x,t) = P_0\left\{P_d^+ e^{ik_1 x} + P_d^- e^{-ik_1 x}\right\} e^{-i\Omega t} \quad (12)$$

$$u'_d(x,t) = \frac{P_0}{\rho_1 a_1}\left\{P_d^+ e^{ik_1 x} - P_d^- e^{-ik_1 x}\right\} e^{-i\Omega t} \quad (13)$$

Region C

$$P_c'(x,t) = P_0 \frac{1}{x+x_v}\left\{P_c^+ e^{ik_1 x} + P_c^- e^{-ik_1 x}\right\} e^{-i\Omega t} \quad (14)$$

$$u_c'(x,t) = \frac{P_0}{\rho_1 a_1}\frac{1}{x+x_v}\left\{P_c^+ e^{ik_1 x} - P_c^- e^{-ik_1 x}\right\} e^{-i\Omega t} \quad (15)$$

The shock reflectance can be calculated from the shock admittance which is calculated from the linear results of Culick and Rogers:

$$\beta_{ISH}^0 = \frac{1+A_{SH}^0}{1-A_{SH}^0} = \frac{P_c^+ e^{-ik_1 x_s}}{P_c^- e^{ik_1 x_s}}. \quad (16)$$

The shock reflectance is given for the shock location at $x = 0$. The exponential terms in (above) contain the correction for the shock located at $x = -x_s$ rather than $x = 0$. The matching at $x = -L_I$ is determined from continuity of mass and pressure.

A simple dump plane area change is a nonisentropic process unless the areas are equal, $S_I = S_C$. However, for a first approximation, an isentropic area change is assumed even though $S_I \neq S_C$. Matching across the dump plane involves mass and pressure continuity given by

$$P_1' = P_2' \quad (17)$$

and

$$u_1' = u_2' \frac{\rho_1}{\rho_2}\frac{S_C}{S_I}. \quad (18)$$

This form of mass continuity requires that the fluctuating entropy not change across the dump plane. (This is the same approximation as used above.) Let

$$\beta_{ISH} = \beta_{ISH}^0 e^{i2k_1 x_s} = \frac{P_c^+}{P_c^-} = \frac{P_d^+}{P_d^-}. \quad (19)$$

and define

$$A_{ISH} = \frac{\beta_{ISH}-1}{\beta_{ISH}+1} \quad (20)$$

to find

$$\beta_I = \frac{P_1^+}{P_1^-} = \frac{\frac{a_d}{a_1}\frac{A_C}{A_I} + A_{ISH}}{\frac{a_d}{a_1}\frac{A_C}{A_I} - A_{ISH}}. \quad (21)$$

Substitute $\frac{a_d}{a_1}$ from the standard equations for isentropic expansion.

2.1.2 Entropy Generation at Shock

The linear shock position is given by $x_s = -\bar{x}_s + x_s'$ from Culick and Rogers [8]

$$x_s' = \left(\frac{C}{1-i\omega\tau}\right) P_c'(-\bar{x}_s) \quad (22)$$

$$C = \frac{-1}{P_{upst}}\left(\frac{1}{S}\frac{dS}{dx}\right)^{-1}\frac{(\gamma+1)^2}{2\gamma(\gamma-1)}\left(1+\frac{\gamma^2+1}{\gamma-1}\bar{M}_{1_s}^2\right)^{-1} \quad (23)$$

$$\tau = \frac{1}{a_{1_s}}\left(\frac{1}{S}\frac{dS}{dx}\right)^{-1}\frac{2(\gamma+1)\bar{M}_{1_s}}{(\gamma-1)}\left(1+\frac{\gamma^2+1}{\gamma-1}\bar{M}_{1_s}^2\right)^{-1} \quad (24)$$

where all terms are calculated at the mean shock location. Here, S represents the area at the shock. From the previous reflectance calculations we find

$$\frac{P_c'(-\bar{x}_s)}{P_1^-} = \left(\frac{x_v - L_I}{x_v - \bar{x}_s}\right)\left(\frac{1}{1+\beta_{ISH}}\right)(\beta_I+1) \\ (\beta_{ISH}e^{-ik_1\bar{x}_s} + e^{ik_1\bar{x}_s})P_0. \quad (25)$$

To determine the fluctuating entropy wave generated at the oscillating shock in a polytropic gas (i.e. $s = c_v \ln(P/\rho^\gamma)$), look at the shock wave in terms of the strength parameter Z (Ref. Whitham "Linear and Nonlinear Waves" [9])

$$Z = \frac{P_2 - P_1}{P_1} = \frac{2\gamma(M^2-1)}{\gamma+1} \quad \text{for} \quad M = \frac{U-u_1}{a_1} \quad (26)$$

and

$$\frac{s_2 - s_1}{c_v} = \ln\left\{(1+Z)\left(1+\frac{\gamma-1}{2\gamma}Z\right)^\gamma\left(1+\frac{\gamma+1}{2\gamma}Z\right)^{-\gamma}\right\} \quad (27)$$

where the subscript 1 is for entering the shock wave and 2 is for leaving the shock. M is the mach number of the flow ahead of the shock relative to the shock.

Consider the shock strength, Z, where P_1 is the mean pressure upstream of the shock and P_2 is the mean pressure downstream of the shock. Assume the inlet flow into the shock is uniform (i.e. $P_1 = P_{10}$). For longer wavelengths (low frequencies) treat $P(x,t)$ as approximately $P(\bar{x},t)$ where $x = \bar{x} + x'$. As long as x' is small then the mean pressure at $x = x' + \bar{x}$ can be expressed in a Taylor series expansion about $x = \bar{x}$. Define Z' so

$$Z = \bar{Z} + Z', \quad (28)$$

$$Z' = \frac{1}{P_{10}(\bar{x})}\left\{P_2'(\bar{x},t) + \left(\frac{dP_{20}(\bar{x})}{dx} - (1+\bar{Z})\frac{dP_{10}(\bar{x})}{dx}\right)x'\right\} \quad (29)$$

$$\text{and} \quad \bar{Z} = \frac{P_{20}(\bar{x}) - P_{10}(\bar{x})}{P_{10}(\bar{x})}. \quad (30)$$

Return to the inlet notation to get

$$Z' = \frac{P_c'(-\bar{x}_s)}{P_{upst}}\left\{1 + Q_1 P_{upst}\frac{1}{S}\frac{dS}{dx}\left(\frac{C}{1-i\omega\tau}\right)\right\} \quad (31)$$

where

$$Q_1 = \left(\frac{\gamma M_{2_s}^2}{1-M_{2_s}^2}\right)\frac{P_{2_s}}{P_{1_s}} - (1+\bar{Z})\left(\frac{\gamma M_{1_s}^2}{1-M_{1_s}^2}\right) \quad (32)$$

and P_{upst} is the mean pressure upstream of the shock. After rearrangement and the expansion of $ln(1+x)$ for small x

$$\frac{s_c'}{c_v} = Z' \cdot Z_{BAR1} \quad (33)$$

where

$$Z_{BAR1} = \frac{1}{1+\bar{Z}} + \frac{\gamma}{\frac{2\gamma}{\gamma-1}+\bar{Z}} - \frac{\gamma}{\frac{2\gamma}{\gamma+1}+\bar{Z}}. \quad (34)$$

Then, assuming the expansion in the diffuser from the shock to the inlet duct is isentropic, it can be shown that

$$\frac{A}{P_1^-} = c_v \frac{P_c'(\bar{x}_s)}{P_1^-} \frac{1}{P_{upst}} Q_2 Z_{BAR1} e^{i\frac{\Omega}{a_0}(x_s)} \qquad (35)$$

where

$$Q_2 = \left\{ 1 + Q_1 P_{upst} \frac{1}{S} \frac{dS}{dx} \left(\frac{C}{1 - i\omega\tau} \right) \right\} . \qquad (36)$$

The result here is that an inlet shock, inlet duct, and dump plane have been reduced to boundary conditions applied at the upstream end of the combustor channel. The boundary conditions are given by 20 and 34. Reducing these components of the inlet to combustor boundary conditions will simplify the characteristic equation for the resonant frequencies.

2.2 Combustor Modeling

The combustor is modeled by matching two acoustic regions across a plane flame as developed by Chu [3]-[6] and shown in Figure 2. The reflectance, β_I, can be coupled with the combustor region from $x = 0$ to $x = x^*$ and the flame matching conditions to determine a new reflectance β_{Iflame} at $x = x^*$. The procedure is similar to defining the inlet reflectance. Also, A is the entropy constant in region 1 (the acoustic region upstream of the flame) and B for region 2 (the acoustic region downstream of the flame). It is assumed that β and A/P^- are known. The equations of P, u, and s in regions 1 and 2 are given by 7-9 and subscripted 1 and 2.

Define β_{Iflame} such that

$$\beta_{Iflame} = \frac{P_2^+}{P_2^-} . \qquad (37)$$

The flame matching conditions at $x = x_f$ are given by Humphrey [10] to be

$$P_1' = P_2' \qquad (38)$$

$$\tilde{G} = W_5 P_1' + W_6 s_1' \qquad (39)$$

$$s_2' = W_9 P_1' + W_{10} s_1' \qquad (40)$$

and $P_{10} = P_{20}$ since the flame is flat and not curved. After some manipulation β_{Iflame} and B/P_2^- can be found as a function of the geometry and the constants W_i.

To avoid confusion we call the reflectance a condensed reflectance when it contains more than just a reflectance and is generally applied at a position other than where the original reflectance occurred. The procedure of this section compresses again the already condensed inlet reflectance at the upstream end of the combustor, β_I, the section of the combustor upstream of the flame, and the flame matching conditions to a new combustor reflectance, β_{Iflame}, applied at $x = x_f$. This sets the boundaries for the combustor to be used in the frequency calculation of the next section. The application of the condensed reflectance does not influence the generality of the linear formulation.

2.2.1 Exit Nozzle Boundary Conditions

The exit boundary conditions require special mention. Often, combustion chambers are terminated by choked nozzles. Marble and Candel [7] showed that incident entropy waves impinging on a choked nozzle would reflect a pressure wave. Hence, a choked exit nozzle has an entropy reflectance as well as an acoustic reflectance. These are linearized results and thus it is proper simply to add the reflected pressure waves. Therefore,

$$P_0 P^- e^{-iKL} e^{-iM_0 KL} = \beta_E P_0 P^+ e^{iKL} e^{-iM_0 KL} + \beta_{EE} \frac{\gamma P_0}{c_p} A e^{i\frac{\Omega}{a_0}L} \qquad (41)$$

where P_0 is dimensional and $P^{\pm}$ are nondimensional terms and β_E is the acoustic nozzle reflectance defined for a nozzle at $x = 0$. The reflectance is the ratio of the reflected to incident wave. (It should be observed that this definition results in a slightly different form for the inlet and exit.) Often the reflectance is given for the case where the boundary is chosen to be at the origin (i.e. $x = 0$) and care must be taken when applying reflectances at locations other than the origin. Define an exit reflectance, β_{Exit}, such that

$$\beta_{Exit} = \frac{P^-}{P^+} . \qquad (42)$$

As a direct consequence of 40 and 41

$$\beta_{Exit} = \frac{\beta_E e^{iKL}}{e^{-iKL} - \beta_{EE} \frac{\gamma}{c_p} \frac{A}{P^-} e^{i\frac{\Omega}{a_0}L} e^{iM_0 KL}} . \qquad (43)$$

It is also common to define the admittance as

$$A_N = \rho_0 a_0 \frac{u'}{P'} . \qquad (44)$$

Using 42 with 7 and 8, 43 becomes

$$A_{NExit} = \frac{K - \beta_E}{K + \beta_E} \qquad (45)$$

where

$$K = 1 - \beta_{EE} \frac{\gamma}{c_p} \frac{A}{P^-} e^{i\frac{\Omega}{a_0}L} e^{iKL} e^{iM_0 KL} . \qquad (46)$$

These definitions assume that the acoustic exit reflectance (defined at $x = 0$), β_E, does not vanish. In the case where the acoustic exit reflectance vanishes it would be necessary to return to 40 and formulate an expression independent of P^+.

2.3 Linear Frequency Calculation

The previous sections reduce the inlet with the inlet shock, the dump plane, and the plane flame to a single set of boundary conditions for the inlet to the combustor. Eliminate P_2^+ and P_2^- with β_{Iflame} and β_{Exit} to

get

$$1 - \beta_{I\,flame}\beta_{Exit} = 0. \qquad (47)$$

Equation 46 is a transcendental equation for the linear resonant frequencies which are the acoustic resonant modes of the *system*. Recall that B/P_1^- is required to calculate β_{Exit} . The resonant frequencies, Ω, are found by solving for the zeroes of 46. For simple cases this can be done analytically but for more typical geometries, 46 is solved numerically. Once the resonant frequencies are known, they can be used to calculate the eigenfunctions and hence the pressure and velocity mode shapes. These calculations are done in the following section for several different cases.

The solution of the equations of acoustics and entropy can be shown to have two distinct modes. These are the classical acoustics mode of acoustic oscillation and the entropy mode of acoustic oscillation. These modes are not discussed in detail here but it is worthy to mention the eigenvalue problem posed contains both modes of oscillation. Hence, the eigenfunctions will contain the standard classical acoustic modes as well as others which are not explained within the context of classical acoustics.

3 Results of Linear Analysis

Four cases are chosen to illustrate physical processes and are identified by Run n, where n is 1, 2, 3, or 4. Run 1 studies the response of the flame to upstream entropy fluctuations. Runs 1-3 all treat the upstream entropy as an input parameter. Run 2 studies the stability of a combustor with no flame but upstream fluctuating entropy and exit entropy reflectance. Run 3 combines the exit entropy reflectance and the plane flame. Again, the upstream entropy is parametrically varied in the stability study. Run 4 uses the linear inlet shock theory to determine the upstream acoustic-entropy coupling. Define the notation that

$$\mathcal{N} = \frac{A}{c_p P_1^-}. \qquad (48)$$

A summary of the mean flow conditions is given for each run in Table 1.

3.1 Run 1 – Response of Flame to Entropy

Run 1 uses typical values for the flame conditions but has all acoustic reflectances set to zero. This simulates a flame in an infinite medium where no acoustic reflectances are present. If a constant fluctuating entropy is generated upstream proportional to the pressure, then the flame will respond so as to reflect and transmit a pressure wave as well as transmit an entropy wave. Thus, the only neutrally stable value of $\mathcal{N}$ (which is the ratio of the magnitude of the entropy wave over the reflected pressure wave) is the one which produces a stable oscillation. A neutrally stable wave has a zero growth rate, $\alpha = 0$. This value of $\mathcal{N}$ was found to be 3.202 (Tables 2 and 3). The neutral growth value of $\mathcal{N}$ can be calculated directly from the analysis presented by Humphrey [10] which produced the same value of $\mathcal{N}$=3.202.

The entropy, A, is the only driving mechanism in this case. Thus to get a neutrally stable reflected pressure wave of 1 psi then an entropy wave must be generated of magnitude $.0128 BTU/lbm/\ ^\circ R$. The frequencies calculated result from entropy generation at the inlet which is proportional to the fluctuating pressure at the inlet. The position of the flame from the inlet along with the mean flow and acoustic velocities determine the frequencies. The position of the flame however does not effect the ratio $\mathcal{N}$.

Although the flame oscillates about its mean position, the motion is very small. Typical magnitudes of flame displacement are of the order $10^{-5} ft$. This justifies the analytical presumption that the acoustic terms into and out of the flame can be evaluated at the mean flame position.

3.2 Run 2 – Response of the Exit Nozzle to Entropy

Run 2 studies the influence of entropy waves impinging upon a choked nozzle on the linear stability. The inlet is taken to be an acoustic wall. The exit has acoustic and entropy reflectance as well as acoustic losses. The magnitude of acoustic-entropy coupling at the inlet, $\mathcal{N}$, is varied. The resonant frequencies are calculated for each value of $\mathcal{N}$ and summarized in Tables 4 and 5. There is a definite selection of frequencies that become unstable while others become more stable for increasing values of $\mathcal{N}$. The first unstable frequencies are 176, 527, 879 Hz and become unstable for $\mathcal{N} > .50$ (at $\mathcal{N} = .50$, $\alpha \approx -.26$). The selection of frequencies to become unstable is determined by the phase of the entropy at the exit nozzle relative to the acoustic pressure.

3.3 Run 3 – Study of $\mathcal{N}$ with Flame

Run 3 takes a typical combustor with an acoustic wall for an inlet and a flame temperature ratio of 4 to study the effects on stability of a plane flame for various values of $\mathcal{N}$. The exit nozzle has acoustic and entropy reflectances with acoustic losses. The eigenvalues were calculated for each $\mathcal{N}$ and are given in Table 6. The first frequency that is observed to become unstable is 705 Hz for $\mathcal{N} > .475$. Other frequencies to become unstable for larger $\mathcal{N}$ are 977, 422, and 232 Hz. The selection of driven frequencies involves the phase relationships between entropy and pressure at the inlet, flame, and exit. All three locations contribute to the stability and have to be considered together to get the stability of each mode. Figure 4 shows the pressure and entropy magnitude mode shape and phase distribution for the frequency 705 Hz. It can be seen from these plots that there is some conversion of energy in the entropy fluctuations to acoustic energy at the flame. This conversion of energy at the flame is one

source of driving and is a function of frequency and local pressure.

3.4 Run 4 – Study $\mathcal{H}$ with an Inlet Shock

Run 4 uses the linear shock theory applied to an inlet duct terminated by an inlet shock to determine the value of the combustor reflectance at $x = 0$. The intent is to approximate a realistic combustor inlet configuration. The value of $\mathcal{H}$ is given as a function of the inlet shock and frequency. The resonant frequencies contain both acoustic and entropy modes and are given in Table 7. From Runs 2 and 3, we find that the magnitude of $\mathcal{H}$ is sufficient to drive the system more vigorously than the decay rates in Table 7 would imply. This suggests that the driving is "out-of-phase" in this case. However, the magnitude of the inlet acoustic reflectance is $\approx 2/3$ where in Runs 2 and 3 it was 1. The shock provides significant damping. Changes in $\mathcal{H}$ and β_I (at $x = 0$) are studied by changing the inlet length. The resonant frequencies are solved for different inlet lengths and given in Table 8.

This particular choice of inlet lengths shows that the eigenvalues are dependent on geometry and frequency. But the driving is never sufficient to push the system into instability. This implies that the linear oscillating shock does not provide a sufficiently large entropy fluctuations to force instability. Figures 5 and 6 show the pressure and entropy magnitude mode shapes and phase distributions for two cases. Figure 5 shows an acoustic mode in which acoustic energy is converted to entropy fluctuations at the flame. Figure 6 shows an entropy mode case where acoustic energy is gained at the flame by reducing the magnitude of the entropy fluctuations.

4 Summary and Conclusions

The linear stability of acoustics with entropy is strongly a function of the entropy even for cases where the frequencies are only slightly modified. The boundary conditions are extremely important and can significantly alter both the stability and the frequencies of oscillation. The application of an inlet shock to the entropy coupling at the inlet is derived and shown to be insufficient to drive the system under the current geometry. It is believed that this is due to an underestimation of the oscillating heat release at the plane flame. It is suggested that the plane flame matching condition be used to develop a variable area multi-dimensional flame sheet. This could greatly enhance the driving at the flame. Then the results with enhanced heat release can be applied to the one-dimensional acoustics.

The differences between acoustic and entropy modes are significant (see Figures 5 and 6). In general, the entropy alters the growth rate more than the frequency. The dependence of frequency upon entropy is more pronounced for the entropy modes than for the acoustic modes.

Acknowledgment

We gratefully acknowledge that this work was supported by the Office of Naval Research through a graduate research fellowship and contract N00014-84-K-0434.

References

[1] D. L. Davis. *Coaxial Dump Combustor Combustion Instabilities, Part 1 - Parametric Test Data.* Technical Report, Aero Propulsion Laboratory, Air Force Wright Aeronautical Laboratories,Wright-Patterson AFB, 1981.

[2] Duane A. Smith. *An Experimental Study of Acoustically Excited, Vortex Driven, Combustion Instability within a Rearward Facing Step Combustor.* PhD thesis, California Institute of Technology, 1985.

[3] B. T. Chu. *Stability of Systems Containing a Heat Source - the Rayleigh Criterion.* Technical Report, National Advisory Committee for Aeronautics, June 1956. Engineering Library, Lockheed Aircraft Corporation. NACA RM 56D27.

[4] B. T. Chu. *Mechanism of Generation of Pressure Waves at Flame Fronts.* Technical Report, National Advisory Committee for Aeronautics, October 1956. NACA TN 3683.

[5] B. T. Chu. On the generation of pressure waves at a plane flame. *Fourth International Symposium on Combustion*, 603–612, 1953.

[6] B. T. Chu. *Pressure Waves Generated by Addition of Heat in a Gaseous Medium.* Technical Report, Johns Hopkins University, June 1955. NACA TN 3411.

[7] Frank E. Marble and Sebastien M. Candel. An analytical study of the non-steady behavior of large combustors. *International Symposium of Combustion*, 1978.

[8] F. E. C. Culick and Tom Rogers. The response of normal shocks in diffusers. *Journal of the American Institute of Aeronautics and Astronautics*, 21(10):1383–1390, August 1980.

[9] G. B. Whitham. *Linear and Nonlinear Waves*, chapter 6. John Wiley and Sons, 1973.

[10] Joseph W. Humphrey. *Linear and Nonlinear Acoustics with Entropy in Combustion Chambers.* PhD thesis, California Institute of Technology, June 1987.

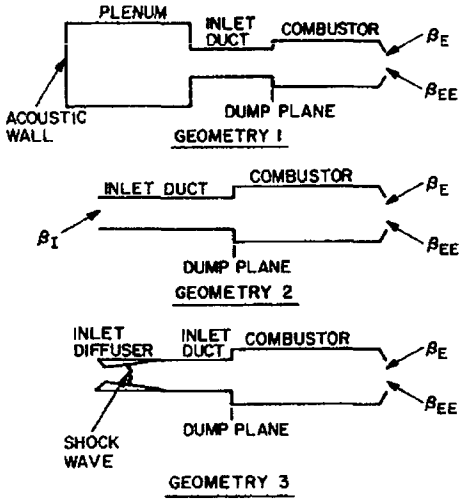

Figure 1: Three Modeling Geometries for One-Dimensional Ramjets.

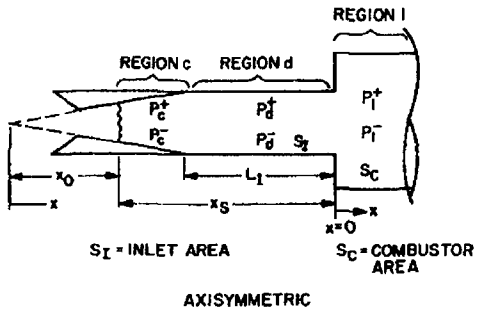

Figure 2: Geometry of Inlet Diffuser and Inlet with Shock.

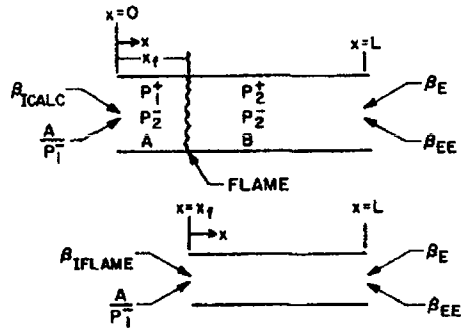

Figure 3: Combustor Model Geometry.

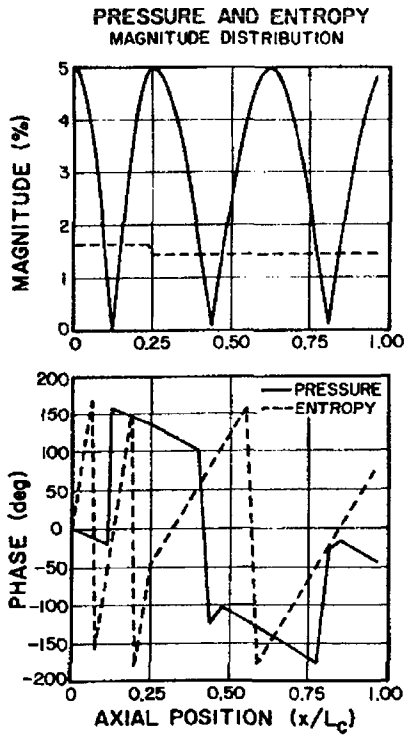

Figure 4: Pressure and Entropy Magnitude Mode Shape and Phase Distribution for Run-3 and $\omega = 705 Hz$.

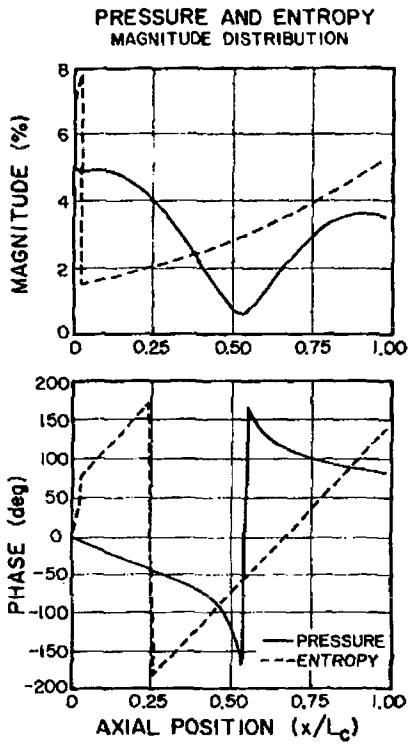

Figure 5: Pressure and Entropy Magnitude Mode Shape and Phase Distribution for Run-4 and $\omega = 315Hz$.

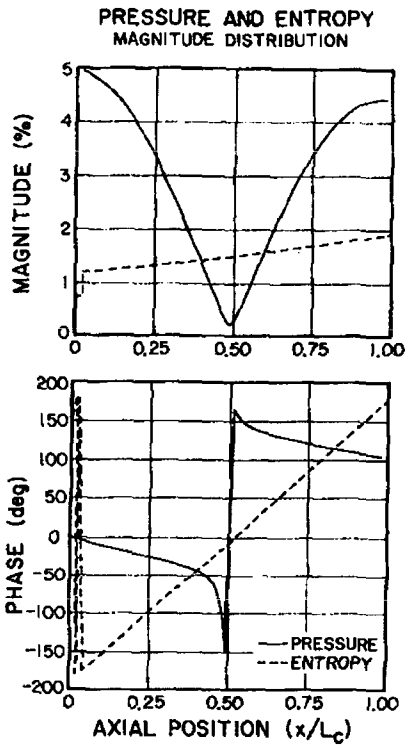

Figure 6: Pressure and Entropy Magnitude Mode Shape and Phase Distribution for Run-4 and $\omega = 377Hz$.

	Run 1	Run 2	Run 3	Run 4
$T_{1_0}\ (°R)$	950	950	950	1000
$P_{1_0}\ (psi)$	75	75	75	75
M_{1_0}	0.25	0.25	0.25	0.20
$L\ (ft)$	4	4	4	4
$c_{p1} = c_{p2}\ (BTU/lbm/°R)$	0.3	0.3	0.3	0.3
γ_1	1.38	1.38	1.38	1.38
γ_2	1.38	1.38	1.28	1.28
β_I	(0,0)	(1,0)	(0,0)	Calculated
β_E	(0,0)	(.909,0)	(.864,0)	(.890,0)
β_{EE}	(0,0)	(-.119,0)	(-.242,0)	(-.196,0)
λ	4	1	4	4
$S_t\ (ft/sec)$	1	1	1	1
a	1.4	1.4	1.4	1.4
b	.1	.1	.1	.1
$x_f = x_{flame}\ (ft)$	1	1	1	.1
$S_0\ (Area(ft^2))$	.083	.083	.083	.083

Table 1: Summary of Mean Conditions for All Four Runs.

$\mathcal{H}$	Ω_1		Ω_2		Ω_3		Ω_4	
	ω	α	ω	α	ω	α	ω	α
$2.5*10^{-5}$	141	-526	422	-526	703	-526	984	-526
$2.5*10^{-4}$	141	-423	422	-423	703	-423	984	-423
$2.5*10^{-3}$	141	-320	422	-320	703	-320	984	-320
$2.5*10^{-2}$	141	-217	422	-217	703	-217	984	-217
$2.5*10^{-1}$	141	-114	422	-114	703	-114	984	-114
2.5	141	-11	422	-11	703	-11	984	-11
$2.5*10^{1}$	141	92	422	92	703	92	984	92

Table 2: Run 1 – Dependence of Frequency and Damping on Entropy.

$x_f(ft)$	Ω_1		Ω_2		Ω_3		Ω_4	
	ω	α	ω	α	ω	α	ω	α
1	141	.001	422	.001	703	.001	984	.001
2	70	.0004	211	.0004	352	.0004	492	.0004

Table 3: Run 1 – Flame Position Dependence for $\mathcal{H} = 3.202$.

$\mathcal{H}$	Ω_1		Ω_2		Ω_3		Ω_4		Ω_5		Ω_6	
	ω_1	α_1	ω_2	α_2	ω_3	α_3	ω_4	α_4	ω_5	α_5	ω_6	α_6
$2.5*10^{-4}$	0	-2.66	176	-2.66	352	-2.66	527	-2.66	703	-2.66	879	-2.66
$2.5*10^{-3}$	0	-2.67	176	-2.65	352	-2.67	527	-2.65	703	-2.67	879	-2.65
$2.5*10^{-2}$	0	-2.80	176	-2.50	352	-2.80	527	-2.50	703	-2.80	879	-2.50
$2.5*10^{-1}$	0	-4.30	176	-1.30	352	-4.30	527	-1.30	703	-4.30	879	-1.30
$1.0*10^{-0}$			176	1.60			527	1.60			879	1.60
$2.5*10^{-0}$			176	5.50			527	5.50			879	5.50

Table 4: Run 2 – Resonant frequencies for Acoustic Modes 1-6 for a Combustor with Entropy Reflectance at the Exit and No Flame.

$\mathcal{H}$	Ω_7		Ω_8		Ω_9		Ω_10		Ω_11		Ω_12	
	ω_7	α_7	ω_8	α_8	ω_9	α_9	ω_10	α_10	ω_11	α_11	ω_12	α_12
$2.5*10^{-4}$	0	-187	117	-187	234	-187	352	-187	469	-187	586	-187
$2.5*10^{-3}$			117	-144	234	-144	352	-144	469	-144	586	-144
$2.5*10^{-2}$	0	-100	117	-101	235	-101	352	-100	468	-101	586	-101
$2.5*10^{-1}$	0	-55	115	-59	236	-59	352	-55	467	-59	588	-59
$1.0*10^{-0}$			113	-35	238	-35			465	-35	590	-35
$2.5*10^{-0}$			112	-21	240	-21			463	-21	591	-21

Table 5: Run 2 – Resonant Frequencies for Entropy Modes 7-12 for a Combustor with Entropy Reflectance at the Exit and No Flame.

$\mathcal{H}$	Ω_1		Ω_2		Ω_3		Ω_4		Ω_5		Ω_6	
	ω_1	α_1	ω_2	α_2	ω_3	α_3	ω_4	α_4	ω_5	α_5	ω_6	α_6
$2.5 * 10^{-3}$	0	-11.0	256	-7.5	447	-8.8	706	-11.3	961	-6.5	323	-310
$2.5 * 10^{-2}$	0	-11.7	256	-7.4	446	-8.7	706	-10.6	961	-6.5	323	-251
$2.5 * 10^{-1}$	0	-19.9	256	-7.3	441	-7.7	706	-4.8	967	-5.6	327	-175
$4.7 * 10^{-1}$	0	-33.8	256	-6.4	437	-5.9	706	-.02	972	-3.4	336	-156
$7.5 * 10^{-1}$	31	-49	256	-4.7	432	-2.6	705	5.0	977	0.6	343	-146
$1.5 * 10^{-0}$	59	-30	256	0.1	422	8.2	705	15.0	880	-62	356	-137
$2.5 * 10^{-0}$	72	-16	256	5.7	417	21.0	705	26.0	876	-46	362	-134

Table 6: Run 3 – Resonant Frequencies 1-6 for Combustor with Entropy Reflectance at Exit and Plane Flame.

Frequency		Reflectance β_I		$\mathcal{H}^*$	
0	-14.0	.6577	.0000	-.0006068	.0000000
315	-23.5	.6157	.0209	-.0006004	.0003414
612	-28.9	.5967	.0111	.0004766	.0003502
925	-21.7	.5943	.0096	.0002163	-.0001738
377	-64.3	.6045	-.0044	.0063566	.0002277

Table 7: Run 4 – Resonant Frequencies and Frequency Dependence of the Inlet Reflectance with Entropy for a Combustor with an Oscillating Shock.

Inlet Duct	Ω_1		Ω_2		Ω_3		Ω_4		Ω_5		Ω_6		Ω_7	
Length														
1.0	0	-15	204	-113	317	-30	607	-29	923	-22			736	-129
2.5	0	-14			315	-24	612	-29	925	-22	377	-64		
4.0	0	-13	228	-59	303	-28	594	-35	925	-20				

Table 8: Run 4 – Frequency Dependence on Shock Position.